Short Ligands Affect Modes of QD Uptake and Elimination in Human Cells

Noura A. Al-Hajaj,[†,§] Alexandre Moquin,[‡,§] Kevin D. Neibert,[†,§] Ghareb M. Soliman,[†,‡] Françoise M. Winnik,[‡,*] and Dusica Maysinger[†,*]

[†]Department of Pharmacology and Therapeutics, McGill University, 3655 Promenade Sir-William-Osler, Room 1314, McIntyre Medical Sciences Building, Montreal, QC, H3G 1Y6, Canada and [‡]Department of Chemistry and Faculty of Pharmacy, Université de Montréal, CP 6128 Succursale Centre Ville, Montréal, QC, H3C 3J7, Canada. [§]These authors contributed equally to this work.

ABSTRACT In order to better understand nanoparticle uptake and elimination mechanisms, we designed a controlled set of small, highly fluorescent quantum dots (QDs) with nearly identical hydrodynamic size (8—10 nm) but with varied short ligand surface functionalization. The properties of functionalized QDs and their modes of uptake and elimination were investigated systematically by asymmetrical flow field—flow fractionation (AF4), confocal fluorescence microscopy, flow cytometry (FACS), and flame atomic absorption (FAA). Using specific inhibitors of cellular uptake and elimination machinery in human embryonic kidney cells (Hek 293) and human hepatocellular carcinoma cells (Hep G2), we showed that QDs of the same size but with different surface properties were predominantly taken up through lipid raft-mediated endocytosis, however, to significantly different extents. The latter observation infers the contribution of additional modes of QD internalization, which include X-AG cysteine transporter for cysteine-functionalized QDs (QD-CYS). We also investigated putative modes of QD elimination and established the contribution of P-glycoprotein (P-gp) transporter in QD efflux. Results from these studies show a strong dependence between the properties of QD-associated small ligands and modes of uptake/elimination in human cells.

KEYWORDS: quantum dot · human Hep G2 · QD uptake · QD elimination · P-glycoprotein · asymmetrical flow-field-flow fractionation

Semiconductor nanocrystals, or quantum dots (QDs), are powerful and versatile fluorescent probes for biomedical imaging and diagnostics, particularly for long-term, multiplexed, and quantitative detection.[1—4] The wide adoption of QDs as imaging tools in biology and medical research stems from the fact that they readily penetrate into cells without losing their unique photophysical properties, in particular, their size-tunable emission, high quantum yield, broad absorption spectrum, and resistance to photobleaching.[5—7] Although successful application of *in vivo* imaging of QDs has been demonstrated in several animal models, their transition in human medicine is hampered by issues related to the safety of human exposure to QDs, since they generally contain highly toxic elements, such as cadmium, tellurium, and selenium.[8—10] One fears that upon long-term sequestration in the liver, kidney, and other organs, QDs will gradually lose their protective cap causing toxic core components to be progressively released.[11] The ambivalence surrounding the potential use of QDs in nanomedicine has prompted intensive efforts directed toward the development of cadmium-free and alternative "safe" QDs.[12] Concerns over QD accumulation *in vivo* have additionally stimulated research aimed at elucidating the processes associated not only with their cellular uptake and intracellular fate but also with their eventual exit from the cells.[12—14]

Recent investigations into the nature of the relationship between cellular uptake and physicochemical properties of QDs indicate that, in the absence of specific interactions, the entry of nanoparticles into cells and their cytosolic access are primarily governed by three factors: size, shape, and surface charge.[15—19] Surface properties at the nanoscale strongly influence not only specific modes of internalization and subsequent subcellular localization, but also molecular and biological processes, including cell division and differentiation, ultimately dictating cellular fate.[20—22] It was also shown that QD internalization can only occur if the concentration of QDs at the plasma membrane is sufficient.[23] The initial contact of QDs with cells, namely, their interactions with the lipid bilayer and the surface proteoglycans, is controlled by the QD charge and concentration.[24] Since the proteoglycans are negatively charged, positively charged QDs are attracted toward the cell membrane by electrostatic interactions and accumulate readily at the plasma membrane, permitting internalization. Neutral or negatively charged QDs are only weakly bound to the lipid

* Address correspondence to francoise.winnik@umontreal.ca, dusica.maysinger@mcgill.ca.

Received for review March 16, 2011 and accepted May 25, 2011.

Published online May 26, 2011
10.1021/nn201009w

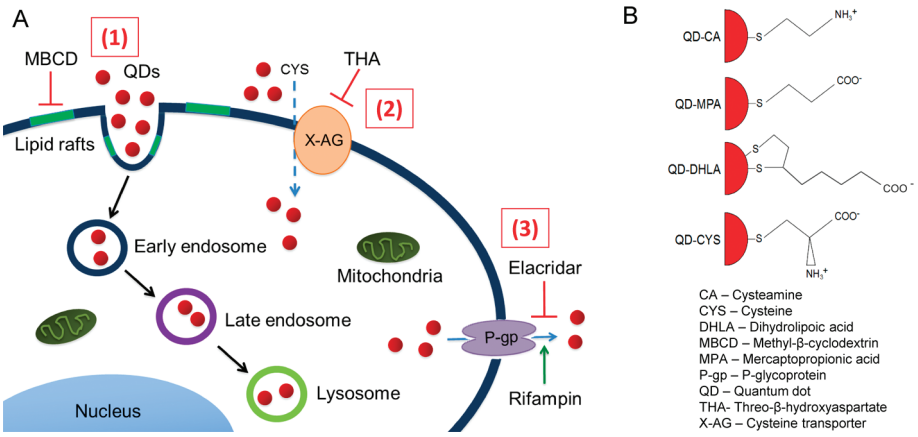

Figure 1. Proposed modes of QD uptake and elimination. (A) Schematic representation of the investigated modes of QD uptake and elimination by (1) lipid raft endocytosis, (2) X-AG cysteine transporter, and (3) P-glycoprotein (P-gp). Pharmacological inhibitors and activators are indicated. (B) Diagram of representative QD structures and list of abbreviations used.

bilayer and thus are less readily taken up.[25] Given their size (4−5 nm in radius), QDs cross the plasma membrane primarily through pinocytosis, a distinct set of endocytosis mechanisms, chiefly responsible for the uptake of cell nutrients and other small particles (<100 nm). The contribution of each endocytosis pathway can be assessed using inhibitors that suppress specific internalization processes.[25−27] Many studies aimed at tracking the fate of internalized QDs by fluorescence imaging have revealed the preferential localization of QDs into lysosomes, a common terminus of several endocytic pathways. During uptake, QDs are internalized into endocytic vesicles which fuse with early endosomes and subsequently with late endosomes and lysosomes.[28,29] These observations, together with evidence from inhibitor-based mechanistic studies, suggest that QDs are primarily internalized *via* lipid raft/caveolae and clathrin-dependent endocytosis.[26] Early endosomes which contain QDs have also been observed to traffic back to the plasma membrane in a process which likely contributes to the QDs' exocytosis.[23] There is no consensus as yet on which of the specific processes leads to cytosolic release of QDs and on the possible involvement of exocytic mediators.

We report here the results of a mechanistic study of the cellular entry/exit pathways of QDs having the same CdSe(CdZnS) core coated with one of four different short ligands, such that their hydrodynamic diameters were nearly identical (8−10 nm). Cellular uptake experiments were performed in two human model cell lines: human embryonic kidney cells (Hek 293) and human hepatocellular carcinoma cells (Hep G2). These cell lines are particularly relevant to internalization and exocytosis studies as injected QDs tend to accumulate preferentially in the kidneys and liver of treated animals.[30] QD internalization was observed by confocal fluorescence microscopy. The extent of QD uptake was estimated by plate-based fluorometry, flow cytometry (FACS), and analysis of intracellular cadmium concentrations using flame atomic absorption (FAA). To investigate the role of specific modes of QD entry and export, experiments were carried out in the presence or absence of a number of pharmacological inhibitors and activators. We focused on QDs functionalized with cysteine ligands (QD-CYS) and compared their internalization *via* the X-AG cysteine transport system and lipid rafts, with that of three other QDs.[31−33] To investigate the role of lipid raft-mediated endocytosis, methyl β-cyclodextrin (MBCD) was used due to its tendency to sequester cholesterol from the plasma membrane, thus disrupting the structure and function of lipid rafts.[34] In view of its high rate and broad substrate range, the P-glycoprotein (P-gp) transporter is likely to be involved in QD elimination.[35] To assess the potential role of P-gp in QD elimination, we used two pharmacological agents, elacridar and rifampin, a P-gp inhibitor and a P-gp inducer, respectively.[36,37] The types of QDs employed and the uptake/elimination mechanisms probed are depicted schematically in Figure 1. This study has uncovered significant differences in the extent and mode of QD uptake/elimination, depending on the surface properties of the QD types tested. It also provides strong evidence for the involvement of the P-gp transporter in the release of QDs from cells.

RESULTS AND DISCUSSION

Preparation and Characterization of the QDs (Figure 2 and Table 1). All QDs were synthesized from a single batch of hydrophobic CdSe(CdZnS) nanoparticles with an average radius of 2.4 nm determined by transmission electron microscopy (TEM) (Figure 2A, left panel), by ligand exchange using either mercaptopropionic acid (MPA), dihydrolipoic acid (DHLA), L-cysteine (CYS), or cysteamine (CA).[38,39]

Anionic ligands (MPA, DHLA) were efficient in keeping the QDs suspended in conditions of physiological pH and salt concentrations (Supporting Table 1,

TABLE 1. Physicochemical Characteristics of Quantum Dots

	λ_{em} (nm)	R_{UV} of CdSe core (nm)	R_{TEM} of core−shell (nm)	R_h by AF4 (nm)	zeta-potential (mV)	% of aggregates
QD-MPA	620	2.4	2.0 ± 0.3	4.24 ± 0.23	−32.8	0.0
QD-DHLA	620	2.4		5.03 ± 0.31	−33.7	1.32
QD-CYS	620	2.4		4.41 ± 0.22	−35.8	0.08
QD-CA	617	2.4		3.99 ± 0.29	+41.9	0.22

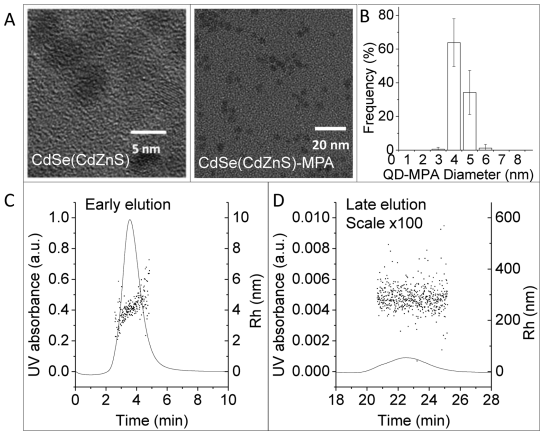

Figure 2. Characterization of QDs. (A) Representative TEM micrographs of unfunctionalized CdSe(CdZnS) QDs (left) and functionalized QD-MPA (right). Scale bars represent 5 and 20 nm, respectively. (B) Normalized size distribution of QD-MPA compiled from several TEM images. (C) Asymmetrical flow field−flow fractionation (AF4) fractograms of QD-CYS (short elution time). (D) Elution of aggregated QD-CYS (long elution time).

Supporting Information). These QDs were stable for 7 days or more, in neutral and mildly acidic conditions. However, none of the QDs were stable in alkaline DMEM conditions due to the presence of high osmolarity of amino acids, salts, *etc*. which caused rapid aggregation of the QDs. The cysteine coating was not as efficient to stabilize the QDs: QD-CYS tend to aggregate after several (∼ 4−5) days in conditions of physiological pH and ionic strength. QD-CA on the other hand were very unstable within pH 4.22−8.6 and aggregated rapidly in the presence of phosphate ions. QD-CAs are only stable in deionized water, any salt in the solution causes them to aggregate over a few hours.

The zeta potential values for QD-MPA, QD-DHLA and QD-CYS (in Milli-Q water) are within −32.8 to −35.8 mV (Supporting Table 1, Supporting Information). The only positively charged QDs are QD-CA (zeta-potential 48.25 mV). Zeta-potential measurements confirmed that, at physiological pH (7.4), QD-MPA, QD-DHLA, and QD-CYS are negatively charged, whereas QD-CA have a positive surface charge (Table 1). When the zeta-potential of the particle falls below a threshold value, the surface charges are no longer strong enough to keep the particles from aggregating and precipitating out of solution. The hydrodynamic radius of the QDs, determined by dynamic light scattering (DLS), is on the order of 4 nm (Supporting Figure 1, Supporting Information), independent of the surface ligand (Table 1).

The QDs were analyzed also by asymmetrical flow field−flow fractionation (AF4) chromatography coupled with UV−visible, fluorescence, multiangle light scattering (MALS), and dynamic light scattering detectors (DLS) (Supporting Figure 2, Supporting Information). Separation of nanoparticles by AF4 occurs according to their size by virtue of their diffusion coefficients in a very thin open channel.[40] Eluting nanoparticles are subjected to a longitudinal carrier flow and an applied field that acts perpendicularly to the length of the channel and causes particles to move toward the accumulation wall. Smaller particles are not affected to the same extent as larger particles. They travel faster than larger particles, resulting in size fractionation of the sample. The eluting fractions are monitored by a UV/vis detector that responds to particle concentration and by a combination of MALS and DLS detectors that yield the particles size.[41] This technique provides the true size distribution of nanoparticles in aqueous media, unlike "batch-mode" DLS which tends to be biased toward the strongly scattering larger particles. The elution profile of a sample of QD-CA monitored by UV/vis detection (λ = 300 nm) is presented in Figure 2C (short elution times) and Figure 2D (long elution times). The most intense band, with an elution time of 4 min, corresponds to the elution of QDs, whereas the weak band between 20 and 26 min is attributed to QD aggregates. Comparison of the areas of the two eluting bands reveals that the fraction of aggregated QDs represents less than 1% of the total QD concentration (Table 1). The elution of QDs was monitored also by MALS and DLS detectors, which yield, respectively, the Rayleigh ratio and the hydrodynamic radius (R_h) of the eluting nanoparticles in fractions. The dots in Figure 2C,D correspond to the R_h values of isolated QD-CA nanoparticles and QD-CA aggregates, respectively. These values were calculated from the diffusion coefficients extracted from the DLS autocorrelated functions determined for each fraction. Data from the fractograms were converted to size distributions represented as plots of the differential weight fractions as a function of R_h (Supporting Figure 2, Supporting Information). The size distributions obtained from AF4 data are narrow in all cases and centered between 4 and 5 nm, depending on the sample. On the basis of these results, we will assume

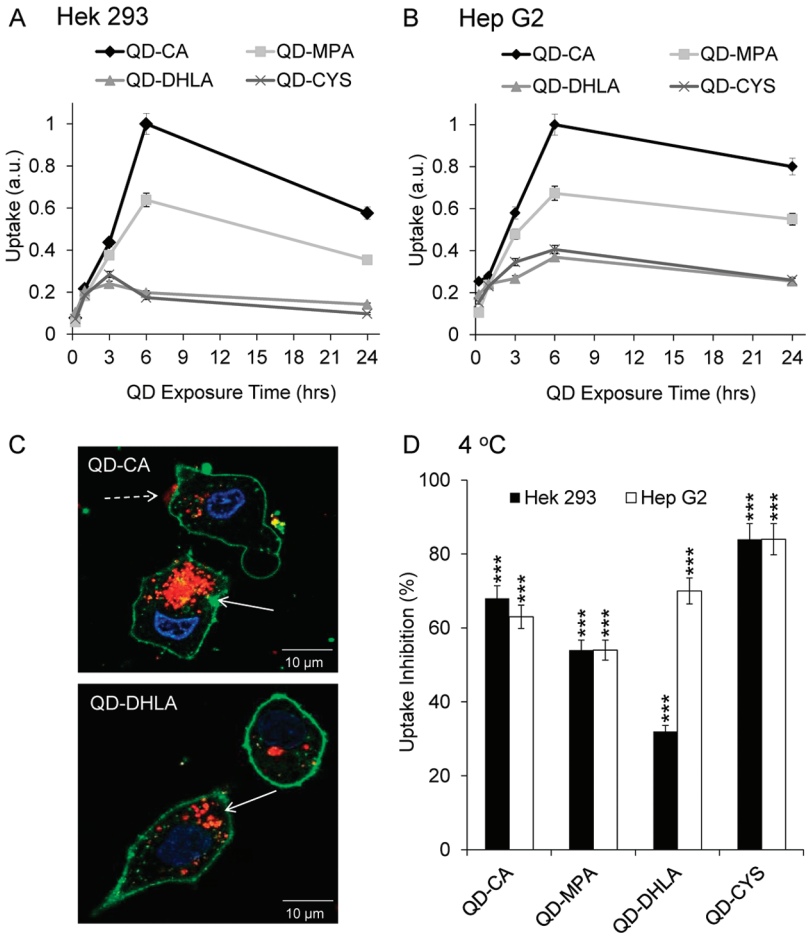

Figure 3. QD uptake by human kidney and liver cells. (A) Hek 293 kidney cells and (B) Hep G2 liver cells were exposed to QDs (100 nM, 1−24 h). Uptake values are the means ± SEM from three independent experiments expressed relative to the maximal QD-CA uptake given 1 au (100 nM; 6 h). (C) Confocal micrographs of QD-CA and QD-DHLA taken up by Hek 293 cells within 1 h. QDs (red), N = nucleus (blue), PM = plasma membrane (green). Dashed arrows indicate partially internalized QDs, and solid arrows indicate fully internalized QDs. Scale bars represent 10 μm. (D) Effect of temperature on QD uptake in Hek 293 cells (black bars) and Hep G2 cells (white bars) exposed to QDs (100 nM; 1 h). The means ± SEM of uptake inhibition (%, at 4 °C) are relative to the uptake of QDs at 37 °C (100%), *** $p < 0.001$.

in the following sections that, in terms of cellular trafficking, the four QD samples have identical size. Such an assumption would have been less justified on the basis of batch-mode DLS data only since size distributions recorded under these conditions are significantly broader (Supporting Figure 1, Supporting Information).

Uptake of QDs by Human Kidney and Liver Cells. QD uptake in human kidney (Hek 293) and liver (Hep G2) cells was assessed spectrofluorometrically (ex/em = 355/612 nm) as a function of time upon exposure to QDs (100 nM). Prior to analysis, cells were washed with acidified buffer solution (phosphate buffer saline, PBS, pH 5.5) for 5 min in order to disrupt weak electrostatic interactions between charged QDs and the plasma membrane and to remove loosely bound and non-internalized QDs from the cell surface.[42] QD uptake in both cell types increased steadily for 6 h but to different extents. Then it remained constant, depending on the cell and QD types (Figure 3A,B). The extent of uptake of positively charged QDs (QD-CA) was significantly higher than that of the negatively charged QDs (QD-CYS, QD-MPA and QD-DHLA) ($p < 0.001$). A similar uptake pattern was found in both cell types at all time points examined. QDs were gradually eliminated over time. There was no significant cytotoxicity of QDs with different ligands within 24 h exposure in both Hek 293 and Hep G2 cell lines (Supporting Figure 3, Supporting Information).

Intracellular cadmium concentrations in cells exposed to QDs were determined by quantitative flame atomic absorption (FAA). Cells exposed to QDs (100 nM) had significantly higher intracellular cadmium concentration compared to those treated with comparable cadmium concentrations in $CdCl_2$ (23.66 μM). For example, Hek 293 cells exposed to QD or $CdCl_2$ for 1 h had intracellular cadmium concentration corresponding to 8.6 ± 0.5 and 0.4 ± 0.4 μM, respectively ($p < 0.001$). These findings suggest that cadmium cations are either less effectively taken in or more rapidly eliminated from the kidney cells than QD (Supporting Figure 4, Supporting Information).

Determining factors influencing the rate and extent of nanoparticles internalization most likely depended

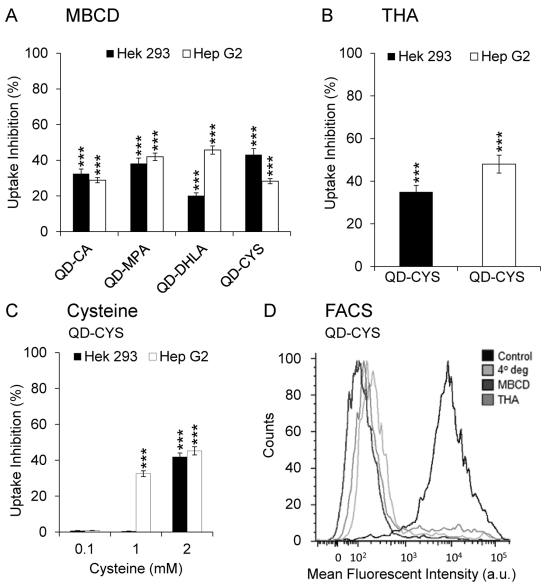

Figure 4. Inhibition of QD uptake in human kidney Hek 293 and liver HepG2 cells: involvement of lipid rafts and the X-AG cysteine transporter. (A) Effect of lipid raft disruption by MBCD (10 mM, 30 min) on QD (100 nM, 3 h) uptake in Hek 293 cells (black bars) and Hep G2 cells (white bars). (B) Effect of cysteine transport inhibition by THA (5 mM, 1 h) on QD-CYS (100 nM, 3 h), and (C) effect of D,L-cysteine (0.1−2 mM, 15 min) on QD-CYS uptake. All values for uptake inhibition (%) in panels A−C are the means ± SEM ($n = 9$), *** $p < 0.001$. (D) Inhibition of QD uptake by MBCD, THA, or at 4 °C measured by flow cytometry (FACS). The scatter histograms are representative of three independent experiments.

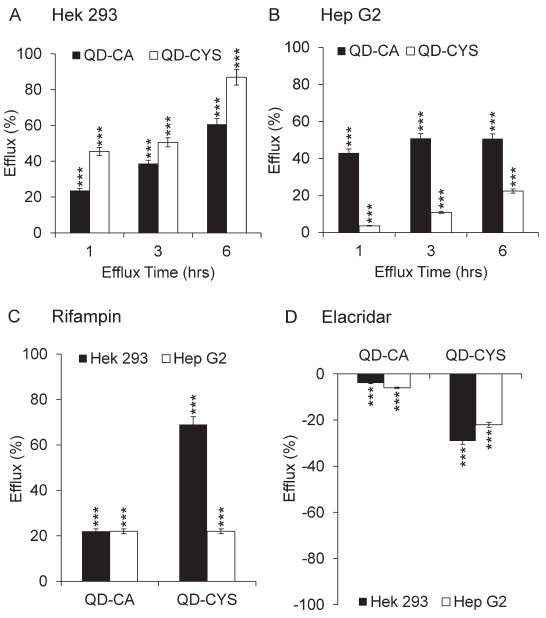

Figure 5. Role of P-gp transporter in QD elimination from human cells. (A) Hek 293 cells and (B) Hep G2 cells were exposed to QDs (100 nM) for 3 h, and QD elimination was measured over time (1−6 h). Data represent the means ± SEM ($n = 9$), *** $p < 0.001$. (C) Activation of P-gp by rifampin (25 μM, 15 h) and elimination of QDs (100 nM). All values (the means ± SEM) represent the change in QD efflux (%) relative to the values from cells exposed to QDs only (no rifampin), *** $p < 0.001$. (D) Inhibition of P-gp by elacridar (50 nM, 1 h) and elimination of QDs (100 nM). Reduction (%) of QD efflux is relative to the efflux in the absence of elacridar. Data points represent the means ± SEM from three independent experiments of triplicates, *** $p < 0.001$.

on the physical and chemical surface properties because the core of all four QD types was similar in size and composition. Interestingly, studies by Stellacci's group show that gold nanoparticles coated with 11-mercapto-1-undecanosulfonate, arranged in subnanometer striations, enter the cells through different routes then those with the same ligand randomly distributed on the gold nanoparticle surface.[43]

To exclude possible artifacts resulting from nonspecific association of the QDs with the cell membrane, we examined the QD localization within live cells using confocal fluorescence microscopy. To facilitate visualization, the plasma membrane and the nucleus were labeled with PHK67 (green) and Hoechst 33342 (blue), respectively. QDs were detected readily by their bright red emission. Representative micrographs recorded upon 1 h treatment of human kidney cells (Hek293) with QD-CA or QD-DHLA are presented in Figure 3C. Both types of QDs were localized predominantly within the cytosol (solid arrow). A small fraction of QD-CA appeared as clusters adhered to the plasma membrane (dashed arrow). These clusters may originate from the small fraction of QD aggregates present in the QD suspension (Table 1 and Figure 2) or from the association of individual QDs on the plasma membrane surface.[23] Due to their size, such aggregates are expected to remain loosely associated with the plasma membrane or enter nonphagocytic cells rather slowly.

Mechanisms Involved in QD Internalization in Hek 293 and Hep G2 Cells. The accumulation of QDs in lysosomal compartments is usually attributed to a mechanism (Figure 1) involving QDs' internalization by endocytosis, trafficking from the plasma membrane by endocytic vesicles, fusion of the vesicles into early endosomes, then late endosomes, and finally fusion with lysosomes.[23] To gain further insight into the mechanisms responsible for the transport of the QDs through the cell membrane, we examined the effect of temperature (Figure 3D) and of pharmacological inhibitors (Figures 4 and 5). QD cellular uptake was determined experimentally by fluorometric measurements. The uptake of all types of QDs by either Hek 293 cells or Hep G2 cells was significantly reduced when the cells were kept at 4 °C, rather than at 37 °C (Figure 3D). The strongest uptake inhibition (~85%) was observed for QD-CYS. Incubation of cells at 4 °C is believed to inhibit the ATP synthase complex, resulting in a reduction of the synthesis of the ATP required for the functioning of the cellular active transport machinery.[44] Exposure to low temperature decreases the fluidity of the lipid bilayer, resulting in a tighter packing of the lipid rafts and other membrane-embedded cholesterol-rich structures.[45] Incubation of cells at low temperature also causes a flattening of caveolae and a blockage of

clathrin-coated pits invagination. These processes effectively inhibit pinocytosis, but their detailed mechanisms are still unclear.[46,47]

Intrigued by the exceptionally strong inhibition of QD-CYS uptake in cells incubated at 4 °C, we undertook a systematic study of two specific active transport mechanisms available for the transport of QD-CYS through the membrane: lipid rafts and the primary sodium-dependent cysteine transporter (X-AG transport system) (see Figure 1). First, to examine the role of lipid-rafts in QD uptake, cells were treated for 30 min with methyl β-cyclodextrin (MBCD, 10 mM), washed, and thereafter incubated with QDs (100 nM) for 3 h. The MBCD pretreatment of the cells, which depletes their membrane cholesterol and disrupts lipid rafts, led to a significant inhibition of QD internalization in Hek 293 cells and Hep G2 cells, compared with cells treated with QDs, but without MBCD (Figure 4A). Furthermore, the extent of QD uptake inhibition depended on the QD surface chemistry and on the cell type. For example, the uptake inhibition of QD-CYS was much more pronounced in Hek 293 cells compared to Hep G2 cells, whereas, in the case of QD-DHLA, the entry was reduced to the greatest extent (46 $\pm$ 4%) in Hep G2 cells compared to Hek 293 (20.2 $\pm$ 3.2%). To test the hypothesis that QDs form specific supramolecular complexes with MBCD, we employed AF4 with MALS/DLS/UV−vis detection due to its sensitivity to small changes in nanoparticle size. AF4 elution profiles of suspensions of QDs preincubated with MCBD are shown in Supporting Figure 5C,D (Supporting Information). A shift of the elution peak, corresponding to an increase in R_h of about 1 nm, was observed in pretreated QD-CYS but not in the case of QD-DHLA. This suggests that complexation occurred between MBCD and QD-CYS but not with QD-DHLA. It is not clear whether or not QD-CYS/MBCD complexation occurred in the living cells, after removal of the excess MBCD prior to QD treatment. To elucidate the mechanisms involved in lipid raft-mediated QD uptake, additional experiments should be performed, such as time lapse measurements of QD−lipid raft interactions and experiments using lipid raft interfering agents other than MBCD. Multiple knockdown and mutation experiments of proteins involved in signaling steps within and downstream from the lipid rafts warrant further investigations to clarify the role of individual components implicated in the QD−lipid raft interactions and internalization process. The structural and functional role of lipid rafts and caveolin in endocytosis of small molecules was recently discussed, and some common mechanisms were proposed.[48,49]

Cysteine, the ligand on the surface of QD-CYS, has a specific transport machinery, the primary sodium-dependent cysteine transporter (X-AG transport system), in both model cell lines selected in this study. Threo-β-hydroxyaspartate (THA), an inhibitor of the X-AG transporter, is a substrate for cysteine, glutamate, and aspartate.[50] We selected THA as a competitive inhibitor of QD-CYS uptake. Hek 293 and Hep G2 cells were treated with THA (5 mM, 1 h), prior to incubation of QD-CYS (100 nM, 3 h) (Figure 4B). Under these conditions, the uptake of QD-CYS was significantly inhibited in Hek 293 cells (35 $\pm$ 4%; ***$p < 0.001$) and in Hep G2 cells (48 $\pm$ 6%; ***$p < 0.001$). To confirm that the cysteine transporter is indeed implicated in QD-CYS internalization, competition experiments with free ligand were performed. Cells in cysteine-free DMEM media were co-treated with D,L-cysteine in concentrations present normally in DMEM (0.1 mM), or in excess (1 and 2 mM) and QD-CYS (100 nM, 15 min) (Figure 4C). Free D,L-cysteine effectively competed with the uptake of QD-CYS in both cell lines, significantly inhibiting internalization in Hek 293 cells (42 $\pm$ 2%; ***$p < 0.001$) and Hep G2 cells (45 $\pm$ 3%; ***$p < 0.001$) cells. Taken together, these observations indicate that the X-AG active cysteine transporter contributes to the internalization of QD-CYS.

To complement the results from the spectrofluorometric determinations, we performed flow cytometry (FACS) (Figure 4D). Following exposure to QD-CYS (100 nM, 3 h, 37 °C, no pretreatment, black lines), FACS histograms revealed a large population of highly fluorescent cells. A decrease of the incubation temperature from 37 to 4 °C or treatment with MBCD and THA significantly reduced the population of fluorescent cells containing QD-CYS, resulting in three almost overlapping peaks with significantly lower mean fluorescence intensities ($p < 0.001$).

Elimination of Multifunctional QDs and the Involvement of P-Glycoprotein. The efflux of QD-CYS and QD-CA from Hek 293 and Hep G2 cells was measured after a 3 h incubation of the cells with QDs (100 nM), followed by aspiration of the cell medium and replacement with fresh medium. The percentages of QD efflux after 1, 3, and 6 h for each cell/QD pair are presented in Figure 5A,B. Significant differences in the fraction of exported QDs were detected depending on the cell type and on the QD surface chemistry. The efflux of QD-CA was greater from Hep G2 cells than from Hek 293 cells within the first 3 h. After 6 h, the percent of QDs left in the cells (~30 to 40%) was similar in both cell lines. The efflux of QD-CYS increased with time for both cell lines, but the efflux from Hep G2 cells was inefficient: after 6 h, nearly 80% of QD-CYS remained trapped within Hep G2 cells, compared to 20% in the case of Hek 293. There are known differences in P-gp activity and expression in the kidneys and liver, pointing to a possible involvement of P-gp in QD elimination.[51]

We used two pharmacological modulators of P-gp activity, rifampin and elacridar, to investigate the role of P-gp in QD elimination. Rifampin is a P-gp inducer known to increase P-gp activity through mechanisms that are still poorly understood.[52] Elacridar is a competitive inhibitor of P-gp that competes with P-gp substrates such as azidopine and inhibits its action.[36] Pretreatment of cells with rifampin (50 nM) for 15 h

resulted in significantly increased QD efflux in both cell lines (Figure 5C), while pretreatment of cells with elacridar (25 μM, 1 h) caused a significant decrease in QD elimination from both cell lines (Figure 5D).

In summary, these studies show how the properties of four functionalized QDs with conserved size but varied surface ligands are differently taken up and eliminated from the human kidney and liver cells. The QDs investigated in the present study were internalized by endocytosis involving lipid rafts in human liver Hep G2 cells and kidney Hek 293 cells. Ligand-specific uptake through the X-AG cysteine transporter was shown to be involved in QD-CYS internalization. In addition, the results suggest a role of P-gp transporter in QD elimination. Further studies are warranted to define signal transduction pathways involved in QD uptake and elimination.

CONCLUSION

Similar to the present studies, P-gps were previously proposed to have a role in the efflux of hydrophobic cytokines, steroid metabolites, and lipids.[35] P-gps have been found within lipid raft membrane domains. Cholesterol was established as one of the modulators of P-gp functions, suggesting the ability of cells to eliminate QDs being, at least in part, dependent on their cholesterol content.[53] It would be interesting to extend these studies by employing cells with knock-downs of enzymes involved in cholesterol synthesis and metabolism as well as physical measurements of membrane stiffness to address the real contribution of cholesterol in QDs' elimination by P-gp. We are currently exploring the role of different proteins involved in QD uptake and elimination by their systematic knock-down in different cell types.

EXPERIMENTAL SECTION

Quantum Dot Preparation. All chemicals were purchased from Sigma-Aldrich unless mentioned otherwise. CdSe(CdZnS) core–shell QDs were synthesized and purified based on a method developed by Pons *et al.*, with some modifications as indicated below.[54] Preparation of precursors: cadmium oxide (n moles) was mixed with tetradecylphosphonic acid (TDPA, 2.05 n moles, from PCI Synthesis) in 1-octadecene (ODE) for a final cadmium concentration of 0.5 M. The mixture was heated to 300 °C and kept at this temperature for 30 min under nitrogen, yielding a white gel with a melting point around 200 °C. Cadmium oleate $Cd(OA)_2$ and zinc oleate $Zn(OA)_2$ were prepared as 0.5 M stock solutions by heating cadmium oxide CdO and zinc oxide ZnO powders in oleic acid at 180 and 240 °C, respectively, for 1 h. The resulting solutions were then degassed at 80 °C under vacuum. Stock solutions of trioctylphosphine sulfide (TOPS 0.5 M) and trioctylphosphine selenide (TOPSe 1.0 M) were prepared by dissolution of sulfur or selenium powders in trioctylphosphine (TOP) at ambient temperature under inert atmosphere, followed by vortex agitation and sonication until all of the solid sulfur/selenium was dissolved.

The cadmium selenide CdSe core nanoparticles were prepared by mixing a solution of Cd(TDPA)2 in ODE (3.2 g, ~2 mmol Cd) with TOP (2 mL), oleylamine (2 mL) and octadecene (5 mL) in a three-neck flask. The preparation was degassed for 30 min under vacuum at 70–80 °C and then heated to 280 °C under nitrogen. A solution of TOPSe (150 μL, 1 M) previously prepared was added to TOP (1 mL) and swiftly injected. The reaction mixture was kept at 230 °C for 10-20 min. The QD growth was controlled by dropwise injection at 1.5 mL/h of TOPSe 1 M. The addition was stopped when the desired QD emission wavelength was obtained (~600 nm). The reaction mixture was cooled to room temperature. The mixture was precipitated in ethanol, centrifuged for 10 min at 8000 rpm and re-suspended in hexanes (9 mL) and TOP (1 mL). The shell of CdZnS was then added by mixing the CdSe core solution in hexanes/TOP (2 mL) with trioctylamine (5 mL) and successively with TOP (0.5 mL), $Cd(OA)_2$ (0.5 M in oleic acid, 0.6 mL) and $Zn(OA)_2$ (0.5 M in oleic acid, 1.2 mL). The mixture was degassed at 70–80 °C for 30 min under vacuum before being heated to 230 °C. TOPS solution (0.5 M in TOP, 1 mL) was then injected dropwise over a few minutes, and the reaction mixture was kept at 230 °C for 30 min or until the desired emission wavelength was obtained. The luminescence intensity increased significantly upon successful formation of the shell. The nanocrystals were precipitated twice in ethanol and re-suspended in 10 mL of chloroform.

QD Surface Modification. Mercaptopropionic acid or dihydrolipoic acid (excess of MPA/DHLA to QDs) was added to a suspension of CdSe(CdZnS) in chloroform. The resulting mixture was heated to 60 °C for 1 h. In the cases of L-cysteine and cysteamine, the ligands were first solubilized in methanol, then mixed with the suspension of QDs and heated to 60 °C for 1 h. The QDs were separated by adding ethanol to the reaction mixture, followed by centrifugation for 5 min at 8000 rpm. A sodium hydroxide solution (0.01 M) was used to resuspend QDs with carboxylic groups (MPA, DHLA, and cysteine) to improve their solubility. QD-CA was readily redispersible in deionized water. The precipitation step with ethanol was repeated, followed by centrifugation for 5 min at 8000 rpm. The precipitates were kept and the ethanol was evaporated under vacuum before resuspending the QDs in either deionized water or aqueous NaOH (0.01 M).

Zeta-Potential Measurements. The zeta-potential of the different QD dispersions was determined at 37 °C by using a Malvern Zetasizer Nano ZS (Worcestershire, UK).

QD Characterization by AF4/UV–Vis/MALS+DLS System. The principle of AF4 has been described elsewhere.[55] An asymmetrical flow field–flow fractionation (AF4) system (AF 2000 MT, Postnova Analytics) with a channel thickness of 350 μm fitted with either a special regenerated cellulose membrane (10 kDa cutoff, RC amphiphilic, Z-MEM-AQU-631, Postnova Analytics) for analysis of positively charged QD-CA or a special polyethylene sulfonate (10 kDa cutoff, PES, Z-MEM-AQU-615, Postnova Analytics) for negatively charged QDs (QD-MPA, QD-DHLA, QD-Cys). The AF4 was connected to a UV–vis variable wavelength spectrophotometric detector (SPD-20A, Postnova Analytics), a fluorescence detector (RF-10A_{XL}, Postnova Analytics), a multiangle light scattering (MALS, Dawn Heleos 8+, Wyatt Technology, Santa Barbara, USA), and a quasi-elastic light scattering (QELS) detector (WyattQELS, Wyatt Technology) which is an add-on unit connected to the 90° angle of the MALS Dawn Heleos 8+ detector. The MALS detector is equipped with a K5 cell and a GaAs laser operating at 658 nm and takes measurements at 0.5 s intervals. Data collection and analysis were done using ASTRA version 5.3.4.20 (Wyatt Technology).

AF4 Separation Conditions. The carrier medium was prefiltered (0.1 μm) deionized water. After flow equilibration, the sample was injected with a flow rate of 0.2 mL/min (injection loop volume: 21.5 μL), followed by a 6 min focusing with a cross-flow rate of 1.5 mL/min and a detector flow rate of 0.5 mL/min. Following a 1 min transition, a two-step cross-flow rate gradient was initiated for the elution mode. The starting cross-flow rate (1.5 mL/min) was decreased linearly to 0 mL/min within 20 min. The cross-flow rate was then kept constant at 0.0 mL/min for 15 min to allow elution of any large aggregates. The detector

flow rate was kept at 0.5 mL/min throughout. All flow rates were controlled by the AF2000 Control software (Postnova Analytics, Salt Lake City, USA). The cross-flow was generated by Khloen syringe pumps (Postnova Analytics), while the axial and focusing flows were delivered by isocratic pumps (Postnova Analytics). The detection of the eluted fractionated QDs/aggregates was performed sequentially by UV absorbance at 300 nm, fluorescence with λ_{ex} 365 nm and λ_{em} 615 nm, MALS, and DLS. Each fractogram presented is representative of a triplicate sample.

QD Characterization by UV−Vis and Spectrofluorometry. Suspensions in water of hydrophilic QDs were diluted to reach an absorbance of the first excitonic peak (~590−600 nm) around 0.1. UV−vis absorbance spectra were recorded on an Agilent diode array spectrophotometer model 8452 A, between wavelengths of 200−800 nm. The empirical formulas proposed by Yu *et al.* were used to determine the diameter and extinction coefficient of cadmium selenide particles from the wavelength of their first excitonic peak (~590 nm).[56] The concentration was then determined using the Beer−Lambert law.

Fluorescence spectroscopy measurements were performed on an Eclipse instrument from Varian Cary. The fluorescence spectra were taken on samples diluted to an absorbance at the excitation wavelength less than 0.1 (monochromator excitation and emission slits were set at 5 nm, photomultiplier voltage was set at 600 V).

Cell Cultures and Treatments. Human embryonic kidney cells (Hek 293) (CRL-1573, ATCC) and human hepatocellular liver carcinoma cells (Hep G2) (HB-8065, ATCC) were cultured in Dulbecco's modified eagle medium (DMEM) (Gibco) containing 10 and 5% of fetal bovine serum (Gibco), respectively. Cells were maintained at 37 °C, 5% CO_2 in a humidified atmosphere. Culture media contained 1% penicillin−streptomycin (Gibco). Cells were grown in serum-containing media for 24 h before cell treatments. Culture medium was then aspirated, cells were washed with PBS (Gibco), QDs and/or drugs were added and incubated at 37 °C for the times indicated. All inhibitors were from Sigma, and the following concentrations and times of incubations were applied: MBCD (10 mM, 30 min), THA (5 mM, 1 h), D,L-cysteine (0.1−2 mM, 15 min), elacridar (50 nM, 1 h), rifampin (25 μM, 15 h). QDs (100 nM) were used in all experiments.

Fluorescence Microscopy Imaging. Cells were seeded at a density of 50 000 cells/well into 8-well chamber slides (Lab-Tek) and incubated with and without QDs (100 nM) for 1 h. Following QD treatment, cells were washed and the nucleus and plasma membranes were stained with 10 μM Hoechst 33342 (Invitrogen) for 1 h and 2 μM PHK67 (Sigma) for 10 min, respectively. Fluorescence micrographs were acquired with a Leica DFC350FX monochrome digital camera connected to a Leica DMI4000B inverted fluorescence microscope using a DAPI-1160A filter at 63× oil immersion (Leica). UV (Hoechst), GFP (PKH), and CYS3 (QD) filters were used, and images were acquired and pseudocolored using Leica Application Suite (LAS).

Determination of QD Uptake by Spectrofluorometry. Cells were seeded at a density of 80 000 cells/well into 96 clear-bottom, black-well plates (Costar) and incubated with and without QDs (100 nM) for the times indicated. Following QD treatment, cells were washed and DMSO was added to each well. Mean fluorescent intensity was measured with a FLUROstar Optima fluorometer (BGM, Labtech) with filters set to ex/em = 355/612 nm and employing 4 × 4 matrix well scanning.

Determination of QD Efflux by Spectrofluorometry. Cells were seeded at a density of 80 000 cells/well into 96 clear-bottom, black-well plates (Costar) and incubated with and without QDs (100 nM) for 3 h. Following QD treatment, cells were washed and fresh serum free media was added to initiate efflux for the times indicated. Cells were then washed, and DMSO was added to each well. Mean fluorescent intensity was measured with a FLUROstar Optima fluorometer (BGM, Labtech) with filters set to ex/em = 355/612 nm and employing 4 × 4 matrix well scanning.

Determination of QD Uptake by Flame Atomic Adsorption (FAA). Standard solutions were prepared by serial diluting 1000 ppm Cd certified standard (SCP Science). Deionized distilled water was used as the diluent and blank. The concentration of cadmium from standard QD solutions (0−100 nM) was measured with a flame atomic absorption spectrophotometer (Perkin-Elmer AAS-700). Hek 293 cells were treated with equimolar concentrations of cadmium, in the form of QDs (100 nM) and $CdCl_2$ (23.66 μM). Following treatment, cells were washed and detached gently by adding PBS containing 0.5% bovine serum albumin (BSA). Cell samples were counted, spun down, and resuspended in deionized distilled water for cadmium determination.

Determination of QD Uptake by Flow Cytometry (FACS). Cells were seeded in 12-well plates (Millipore). Following QD treatment, cells were washed and detached gently by adding PBS containing 0.5% BSA. Samples were collected and analyzed by FACSAria Sorter (BD Biosciences) using PE-Texas Red (ex = 594 nm) filter and expressed as mean fluorescence intensity.

Statistical Analysis. Data were analyzed using SYSTAT 10 (SPSS). Statistical significance was determined by analysis of variance (ANOVA) followed by post hoc, Dunnett's test, independent *t*-test or by one sample *t*-test where specified. Significant differences are indicated by * $p < 0.05$, ** $p < 0.01$, and *** $p < 0.001$.

Acknowledgment. The authors would like to acknowledge the Natural Sciences and Engineering Research Council of Canada (NSERC) and the Canadian Institutes of Health Research (CIHR) for their financial support.

Supporting Information Available: Additional experimental results as mentioned in the text are provided as Supporting Information. This material is available free of charge *via* the Internet at http://pubs.acs.org.

REFERENCES AND NOTES

1. Ho, Y. P.; Leong, K. W. Quantum Dot-Based Theranostics. *Nanoscale* **2009**, *2*, 60–68.
2. Chan, W. C.; Maxwell, D. J.; Gao, X.; Bailey, R. E.; Han, M.; Nie, S. Luminescent Quantum Dots for Multiplexed Biological Detection and Imaging. *Curr. Opin. Biotechnol.* **2002**, *13*, 40–46.
3. Michalet, X.; Pinaud, F. F.; Bentolila, L. A.; Tsay, J. M.; Doose, S.; Li, J. J.; Sundaresan, G.; Wu, A. M.; Gambhir, S. S.; Weiss, S. Quantum Dots for Live Cells, *In Vivo* Imaging, and Diagnostics. *Science* **2005**, *307*, 538–544.
4. Wang, Y.; Chen, L. Quantum Dots, Lighting up the Research and Development of Nanomedicine. *Nanomedicine* **2011**.
5. Hutter, E.; Maysinger, D. Gold Nanoparticles and Quantum Dots for Bioimaging. *Microsc. Res. Tech.* **2010**.
6. Aswathy, R. G.; Yoshida, Y.; Maekawa, T.; Kumar, D. S. Near-Infrared Quantum Dots for Deep Tissue Imaging. *Anal. Bioanal. Chem.* **2010**, *397*, 1417–1435.
7. Wang, C.; Gao, X.; Su, X. *In Vitro* and *In Vivo* Imaging with Quantum Dots. *Anal. Bioanal. Chem.* **2010**, *397*, 1397–1415.
8. Jain, M. P.; Choi, A. O.; Neibert, K. D.; Maysinger, D. Probing and Preventing Quantum Dot-Induced Cytotoxicity with Multimodal α-Lipoic Acid in Multiple Dimensions of the Peripheral Nervous System. *Nanomedicine* **2009**, *4*, 277–290.
9. Lovric, J.; Cho, S. J.; Winnik, F. M.; Maysinger, D. Unmodified Cadmium Telluride Quantum Dots Induce Reactive Oxygen Species Formation Leading to Multiple Organelle Damage and Cell Death. *Chem. Biol.* **2005**, *12*, 1227–1234.
10. Pelley, J. L.; Daar, A. S.; Saner, M. A. State of Academic Knowledge on Toxicity and Biological Fate of Quantum Dots. *Toxicol. Sci.* **2009**, *112*, 276–296.
11. Alexis, F.; Pridgen, E.; Molnar, L. K.; Farokhzad, O. C. Factors Affecting the Clearance and Biodistribution of Polymeric Nanoparticles. *Mol. Pharm.* **2008**, *5*, 505–515.
12. Pons, T.; Pic, E.; Lequeux, N.; Cassette, E.; Bezdetnaya, L.; Guillemin, F.; Marchal, F.; Dubertret, B. Cadmium-Free $CuInS_2$/ZnS Quantum Dots for Sentinel Lymph Node Imaging with Reduced Toxicity. *ACS Nano* **2010**, *4*, 2531–2538.

13. Maysinger, D.; Lovric, J.; Eisenberg, A.; Savic, R. Fate of Micelles and Quantum Dots in Cells. *Eur. J. Pharm. Biopharm.* **2007**, *65*, 270–281.
14. Meng, H.; Liong, M.; Xia, T.; Li, Z.; Ji, Z.; Zink, J. I.; Nel, A. E. Engineered Design of Mesoporous Silica Nanoparticles To Deliver Doxorubicin and P-Glycoprotein SiRNA To Overcome Drug Resistance in a Cancer Cell Line. *ACS Nano* **2010**, *4*, 4539–4550.
15. Mailander, V.; Landfester, K. Interaction of Nanoparticles with Cells. *Biomacromolecules* **2009**, *10*, 2379–2400.
16. Verma, A.; Stellacci, F. Effect of Surface Properties on Nanoparticle−Cell Interactions. *Small* **2010**, *6*, 12–21.
17. Jiang, W.; Kim, B. Y.; Rutka, J. T.; Chan, W. C. Nanoparticle-Mediated Cellular Response Is Size-Dependent. *Nat. Nanotechnol.* **2008**, *3*, 145–150.
18. Gratton, S. E.; Ropp, P. A.; Pohlhaus, P. D.; Luft, J. C.; Madden, V. J.; Napier, M. E.; Desimone, J. M. The Effect of Particle Design on Cellular Internalization Pathways. *Proc. Natl. Acad. Sci. U.S.A.* **2008**, *105*, 11613–11618.
19. Hillaireau, H.; Couvreur, P. Nanocarriers' Entry into the Cell: Relevance to Drug Delivery. *Cell. Mol. Life Sci.* **2009**, *66*, 2873–2896.
20. Asati, A.; Santra, S.; Kaittanis, C.; Perez, J. M. Surface-Charge-Dependent Cell Localization and Cytotoxicity of Cerium Oxide Nanoparticles. *ACS Nano* **2010**, *4*, 5321–5331.
21. Variola, F.; Brunski, J. B.; Orsini, G.; Tambasco De Oliveira, P.; Wazen, R.; Nanci, A. Nanoscale Surface Modifications of Medically Relevant Metals: State-of-the Art and Perspectives. *Nanoscale* **2011**, *3*, 335–353.
22. Zhao, F.; Zhao, Y.; Liu, Y.; Chang, X.; Chen, C. Cellular Uptake, Intracellular Trafficking, and Cytotoxicity of Nanomaterials. *Small* **2011**, *7*, 1322–1337.
23. Jiang, X.; Rocker, C.; Hafner, M.; Brandholt, S.; Dorlich, R. M.; Nienhaus, G. U. Endo- and Exocytosis of Zwitterionic Quantum Dot Nanoparticles by Live HeLa Cells. *ACS Nano* **2010**, *4*, 6787–6797.
24. Nel, A. E.; Madler, L.; Velegol, D.; Xia, T.; Hoek, E. M.; Somasundaran, P.; Klaessig, F.; Castranova, V.; Thompson, M. Understanding Biophysicochemical Interactions at the Nano-Bio Interface. *Nat. Mater.* **2009**, *8*, 543–557.
25. Xiao, Y.; Forry, S. P.; Gao, X.; Holbrook, R. D.; Telford, W. G.; Tona, A. Dynamics and Mechanisms of Quantum Dot Nanoparticle Cellular Uptake. *J. Nanobiotechnol.* **2010**, *8*, 1–13.
26. Zhang, L. W.; Monteiro-Riviere, N. A. Mechanisms of Quantum Dot Nanoparticle Cellular Uptake. *Toxicol. Sci.* **2009**, *110*, 138–155.
27. Richardson, S. C.; Wallom, K. L.; Ferguson, E. L.; Deacon, S. P.; Davies, M. W.; Powell, A. J.; Piper, R. C.; Duncan, R. The Use of Fluorescence Microscopy To Define Polymer Localisation to the Late Endocytic Compartments in Cells That Are Targets for Drug Delivery. *J. Controlled Release* **2008**, *127*, 1–11.
28. Behrendt, M.; Sandros, M. G.; Mckinney, R. A.; Mcdonald, K.; Przybytkowski, E.; Tabrizian, M.; Maysinger, D. Imaging and Organelle Distribution of Fluorescent InGaP/ZnS Nanoparticles in Glial Cells. *Nanomedicine* **2009**, *4*, 747–761.
29. Stern, S. T.; Zolnik, B. S.; Mcleland, C. B.; Clogston, J.; Zheng, J.; Mcneil, S. E. Induction of Autophagy in Porcine Kidney Cells by Quantum Dots: A Common Cellular Response to Nanomaterials? *Toxicol. Sci.* **2008**, *106*, 140–152.
30. Choi, H. S.; Ipe, B. I.; Misra, P.; Lee, J. H.; Bawendi, M. G.; Frangioni, J. V. Tissue- and Organ-Selective Biodistribution of NIR Fluorescent Quantum Dots. *Nano Lett.* **2009**, *9*, 2354–2359.
31. Choi, H. S.; Liu, W.; Misra, P.; Tanaka, E.; Zimmer, J. P.; Itty Ipe, B.; Bawendi, M. G.; Frangioni, J. V. Renal Clearance of Quantum Dots. *Nat. Biotechnol.* **2007**, *25*, 1165–1170.
32. Mahto, S. K.; Park, C.; Yoon, T. H.; Rhee, S. W. Assessment of Cytocompatibility of Surface-Modified CdSe/ZnSe Quantum Dots for Balb/3t3 Fibroblast Cells. *Toxicol. In Vitro* **2010**, *24*, 1070–1077.
33. Idowua, M.; Lamprechta, E.; Nyokong, T. Interaction of Water-Soluble Thiol Capped CdTe Quantum Dots and Bovine Serum Albumin. *J. Photochem. Photobiol., A* **2008**, *198*, 7–12.
34. Ivanov, A. I. Pharmacological Inhibition of Endocytic Pathways: Is It Specific Enough To Be Useful? *Methods Mol. Biol.* **2008**, *440*, 15–33.
35. Orlowski, S.; Martin, S.; Escargueil, A. P-Glycoprotein and 'Lipid Rafts': Some Ambiguous Mutual Relationships (Floating on Them, Building Them or Meeting Them by Chance?). *Cell. Mol. Life Sci.* **2006**, *63*, 1038–1059.
36. Hyafil, F.; Vergely, C.; Du Vignaud, P.; Grand-Perret, T. *In Vitro* and *In Vivo* Reversal of Multidrug Resistance by Gf120918, an Acridonecarboxamide Derivative. *Cancer Res.* **1993**, *53*, 4595–4602.
37. Geick, A.; Eichelbaum, M.; Burk, O. Nuclear Receptor Response Elements Mediate Induction of Intestinal Mdr1 by Rifampin. *J. Biol. Chem.* **2001**, *276*, 14581–14587.
38. Chan, W. C.; Nie, S. Quantum Dot Bioconjugates for Ultrasensitive Nonisotopic Detection. *Science* **1998**, *281*, 2016–2018.
39. Clapp, A. R.; Goldman, E. R.; Mattoussi, H. Capping of CdSe−ZnS Quantum Dots with DHLA and Subsequent Conjugation with Proteins. *Nat. Protoc.* **2006**, *1*, 1258–1266.
40. Giddings, J. C. Field-Flow Fractionation: Analysis of Macromolecular, Colloidal, and Particulate Materials. *Science* **1993**, *260*, 1456–1465.
41. Fraunhofer, W.; Winter, G. The Use of Asymmetrical Flow Field−Flow Fractionation in Pharmaceutics and Biopharmaceutics. *Eur. J. Pharm. Biopharm.* **2004**, *58*, 369–383.
42. Payne, C. K.; Jones, S. A.; Chen, C.; Zhuang, X. Internalization and Trafficking of Cell Surface Proteoglycans and Proteoglycan-Binding Ligands. *Traffic* **2007**, *8*, 389–401.
43. Verma, A.; Uzun, O.; Hu, Y.; Han, H. S.; Watson, N.; Chen, S.; Irvine, D. J.; Stellacci, F. Surface-Structure-Regulated Cell-Membrane Penetration by Monolayer-Protected Nanoparticles. *Nat. Mater.* **2008**, *7*, 588–595.
44. Furuike, S.; Adachi, K.; Sakaki, N.; Shimo-Kon, R.; Itoh, H.; Muneyuki, E.; Yoshida, M.; Kinosita, K., Jr. Temperature Dependence of the Rotation and Hydrolysis Activities of F1-ATPase. *Biophys. J.* **2008**, *95*, 761–770.
45. Van Dooremalen, C.; Koekkoek, J.; Ellers, J. Temperature-Induced Plasticity in Membrane and Storage Lipid Composition: Thermal Reaction Norms across Five Different Temperatures. *J. Insect. Physiol.* **2011**, *57*, 285–291.
46. Banerji, S. K.; Hayes, M. A. Examination of Nonendocytotic Bulk Transport of Nanoparticles across Phospholipid Membranes. *Langmuir* **2007**, *23*, 3305–3313.
47. Chang, E.; Thekkek, N.; Yu, W. W.; Colvin, V. L.; Drezek, R. Evaluation of Quantum Dot Cytotoxicity Based on Intracellular Uptake. *Small* **2006**, *2*, 1412–1417.
48. Parton, R. G.; Richards, A. A. Lipid Rafts and Caveolae as Portals for Endocytosis: New Insights and Common Mechanisms. *Traffic* **2003**, *4*, 724–738.
49. Lajoie, P.; Nabi, I. R. Lipid Rafts, Caveolae, and Their Endocytosis. *Int. Rev. Cell Mol. Biol.* **2010**, *282*, 135–163.
50. Fleck, C.; Schwertfeger, M.; Taylor, P. M. Regulation of Renal Amino Acid (Aa) Transport by Hormones, Drugs and Xenobiotics: A Review. *Amino Acids* **2003**, *24*, 347–374.
51. Kato, R.; Moriguchi, J.; Irie, T.; Nakagawa, M.; Kusukawa, Y.; Matsumura, H.; Ijiri, Y.; Tanaka, K. Effects of Lipopolysaccharide on P-Glycoprotein Expression and Activity in the Liver and Kidneys. *Eur. J. Pharmacol.* **2010**, *636*, 155–158.
52. Matheny, C. J.; Ali, R. Y.; Yang, X.; Pollack, G. M. Effect of Prototypical Inducing Agents on P-Glycoprotein and Cyp3a Expression in Mouse Tissues. *Drug Metab. Dispos.* **2004**, *32*, 1008–1014.
53. Luker, G. D.; Pica, C. M.; Kumar, A. S.; Covey, D. F.; Piwnica-Worms, D. Effects of Cholesterol and Enantiomeric Cholesterol on P-Glycoprotein Localization and Function in Low-Density Membrane Domains. *Biochemistry* **2000**, *39*, 7651–7661.
54. Pons, T.; Lequeux, N.; Mahler, B.; Sasnouski, S.; Fragola, A.; Dubertret, B. Synthesis of Near-Infrared-Emitting, Water-Soluble CdTeSe/CdZnS Core/Shell Quantum Dots. *Chem. Mater.* **2009**, *21*, 1418–1424.

55. Rameshwar, T.; Samal, S.; Lee, S.; Kim, S.; Cho, J.; Kim, I. S. Determination of the Size of Water-Soluble Nanoparticles and Quantum Dots by Field-Flow Fractionation. *J. Nanosci. Nanotechnol.* **2006**, *6*, 2461–2467.
56. Yu, W. W.; Qu, L.; Guo, W.; Peng, X. Experimental Determination of the Extinction Coefficient of CdTe, CdSe, and CdS Nanocrystals. *Chem. Mater.* **2003**, *15*, 2854–2860.